Computers & Fluids, Volume 39, Issue 9, October 2010, Pages 1685-1695

Accepted Manuscript

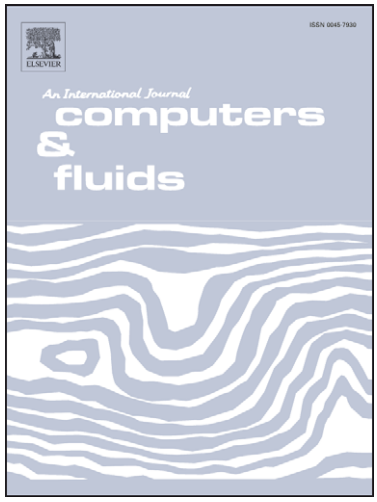

Les Of Intermittency In A Turbulent Round Jet With Different Inlet Conditions

K.K.J. Ranga Dinesh, A.M. Savill, K.W. Jenkins, M.P. Kirkpatrick

PII: S0045-7930(10)00135-0
DOI: 10.1016/j.compfluid.2010.06.004
Reference: CAF 1305

To appear in: *Computers & Fluids*

Received Date: 16 November 2009
Revised Date: 20 April 2010
Accepted Date: 3 June 2010

Please cite this article as: Ranga Dinesh, K.K.J., Savill, A.M., Jenkins, K.W., Kirkpatrick, M.P., Les Of Intermittency In A Turbulent Round Jet With Different Inlet Conditions, *Computers & Fluids* (2010), doi: 10.1016/j.compfluid.2010.06.004

LES OF INTERMITTENCY IN A TURBULENT ROUND JET WITH DIFFERENT INLET CONDITIONS

K.K.J.Ranga Dinesh [1], A.M.Savill [1], K.W.Jenkins [1], M.P.Kirkpatrick [2]

[1] School of Engineering, Cranfield University, Cranfield, Bedford, MK43 0AL, UK

[2] School of Aerospace, Mechanical and Mechatronic Engineering, The University of Sydney, Sydney, LSW2006, Australia

Corresponding author: K.K.J.Ranga Dinesh

Email address: Ranga.Dinesh@Cranfield.ac.uk

Postal Address: School of Engineering, Cranfield University, Cranfield, Bedford, MK43 0AL, UK.

Telephone number: +44 (0) 1234750111 ext 5350

Fax number: +44 1234750195

Second Revised Manuscript prepared for the Journal of Computers and Fluids

20th of April

LES of Intermittency in a Turbulent Round Jet with Different Inlet Conditions

K.K.J.Ranga Dinesh, A.M.Savill, K.W.Jenkins M.P.Kirkpatrick

ABSTRACT

Large eddy simulation (LES) is a promising technique for accurate prediction of turbulent free shear flows in a wide range of applications. Here the LES technique has been applied to study the intermittency in a high Reynolds number turbulent jet with and without a bluff body. The objective of this work is to study the turbulence intermittency of velocity and scalar fields and its variation with respect to different inlet conditions. Probability density function distributions (pdf) of instantaneous mixture fraction and velocity have been created from which the intermittency has been calculated. The time averaged statistical results for a round jet are first discussed and comparisons of velocity and passive scalar fields between LES calculations and experimental measurements are seen to be good. The calculated probability density distributions show changes from a Gaussian to a delta function with increased radial distance from the jet centreline. The effect of introducing a bluff body into the core flow at the inlet changes the structure of pdfs, but the variation from Gaussian to delta distribution is similar to the jet case. However, the radial variation of the intermittency indicates differences between the results with and without a bluff body at axial locations due the recirculation zone created by the bluff body.

Key words: Intermittency, Probability density function, Turbulence, Recirculation, LES

1. INTRODUCTION

Turbulent intermittency is an important issue for many fundamental and practical flows. For example inhomogeneous turbulent free jets, the ignition of turbulent flows, boundary layers and shear layers can exhibit varying levels of turbulent intermittency depending on the conditions adopted for the configurations. A turbulent free round jet issuing from a circular orifice displays intermittent behaviour in the region near the outer edge of the flow and thus can be considered as one of the simple prototype problems for turbulent intermittency. High Reynolds number turbulent jets commonly appear in many engineering application areas such as combustion, propulsion, aeroacoustics, etc. Literature includes various publications which reveal many key physical insights into turbulent jets, such as mixing of active and passive scalars, self-similarity behaviour, skewness and correlations etc. (see [1] for example). A series of intermittency investigations have also been carried out for such shear flows. For example, Townsend [2] investigated the velocity intermittency in a turbulent wake, and Becker et al. [3] have presented intermittency data for the scalar in turbulent jets. Wygnanski and Fiedler [4] also obtained intermittency data for a self-preserving high Reynolds number axisymmetric turbulent jet. Bilger et al. [5] investigated the temperature intermittency using a probability density function approach while Shefer and Dibble [6] reported intermittency as a function of time for the mixture fraction for a propane round jet. Theoretical analyses of turbulent intermittency have also been carried out by Libby [7], Dopazo [8], Chevray and Tutu [9] and many others.

Although accurate numerical calculations of turbulent flows in complex practical situations using engineering models remains a somewhat elusive goal, it has become possible to study prototype problems by means of numerical simulation to help us

identify the physical insights which are often not possible to discover from available experimental techniques. Therefore state-of-art numerical tools can be used to simulate intermittency while available experimental data can be used principally for accuracy tests of the prediction. With recent advances in computer processing techniques and speed, applications of Direct Numerical Simulation (DNS) and Large Eddy Simulation (LES) techniques have become feasible especially in more fundamental investigations. In DNS, all the length and time scales of turbulence are directly resolved and hence no turbulence models are required. In LES, large scales of turbulence are directly computed with the effect of the small scales requiring a turbulence model.

In the last few years comprehensive DNS and LES studies have been carried out with much success for turbulent jets. The first DNS of a spatially evolving turbulent jet was done by Boersma [10]. Freund et al. [11] carried out the first DNS calculations for a compressible supersonic jet and estimated the overall sound pressure levels for aeroacoustic calculations. Lubbers et al. [12] extended Boersma's work and simulated the mixing of a passive scalar using DNS. Babu and Mahesh [13] performed DNS of a spatially evolving round jet with upstream entrainment near the inflow nozzle and demonstrated the importance of allowing inflow entrainment particularly for the studies of near field behaviour. Babu and Mahesh [14] further extended their DNS calculations to study passive scalar mixing for a turbulent round jet which discussed the convective and diffusive dominant regions.

The LES technique allows the simulation of higher Reynolds number jets and many such investigations have now been conducted successfully using the affordable

computing power, eg. see recent reviews [15-16]. Furthermore, Mankbadi et al. [17] have simulated the structure of a supersonic round jet and its sound field using LES. Boersma and Lele [18] have performed LES computations for a compressible round jet, while Yuan et al. [19] reported a series of LES calculations of a round jet issuing normally into a cross flow.

The study of turbulent intermittency is important for many applications such as boundary layer transition in modern turbines and aerofoils, ignition of combustion devices and environmental emissions. However, the majority of existing turbulence models were originally derived for fully developed flows and thus exhibit some deficiencies in the inhomogeneous intermittent regions near the outer edge of such flows which contain regions of irrotational flow. To date only a little work has been done to simulate the intermittency fields of high Reynolds number turbulent round jets and most previous numerical investigations have been carried out using the classical Reynolds averaged Navier-Stokes (RANS) approach. For example, a $k-\varepsilon$ model based intermittency model was developed by Byggstoyl and Kollomann [20] and Kollmann and Janicka [21] studied the intermittency using a transported probability density function (PDF). Cho and Chung [22] developed a more economical intermittency model by incorporating an intermittency transport equation into an already existing $k-\varepsilon$ turbulence model. Several groups extended the Cho and Chung [22] intermittency model and applied this to different applications such as an axisymmetric plume [23], and a plane plume [24]. Pope [25] also calculated intermittency using a velocity-composition transported PDF and Savill [26] discussed the development of a Reynolds stress intermittency transport model for predicting intermittency in transitional flows which was subsequently used successfully by

Alvani [27] to improve PDF predictions for pre-ignition mixing of combusting ignitability.

To further improve the understanding of the intermittency process for more practically oriented engineering problems, it is important to gain more insights into the turbulent intermittency especially for high Reynolds number flows such as turbulent jets. This paper has two objectives. The first objective is to investigate the intermittency for a high Reynolds number round jet and the second objective is to study the intermittency for a jet with a recirculation zone in the near field using the large eddy simulation technique. Therefore the present work aims to improve our knowledge of LES based intermittency prediction for turbulent round jets with and without a recirculation zone, with a view to improvement of LES based sub-grid models to tackle the intermittency explicitly

This paper is organised as follows: in section 2, we discuss the governing equations and modelling. In section 3, we give a detailed description about the numerical setup for simulations. Section 4 first discusses the comparisons of LES results with experimental data and then analyse the probability density functions and intermittency profiles for both velocity and passive scalar fields. Finally, we end the paper with conclusions in section 5.

2. GOVERNING EQUATIONS AND MODELLING

In LES we separate the large energy containing eddies by applying a spatial filter and resolve only large eddies while modelling the small (sub-grid) eddy structures. The governing equations are the spatially filtered incompressible mass, momentum and passive scalar equations and can be written as:

$$\frac{\partial \overline{u}_j}{\partial x_j} = 0, \tag{1}$$

$$\frac{\partial \overline{u}_i}{\partial t} + \frac{\partial (\overline{u}_i \overline{u}_j)}{\partial x_j} = -\frac{1}{\rho}\frac{\partial \overline{P}}{\partial x_i} + \frac{\partial (2\nu \overline{S}_{ij})}{\partial x_j} - \frac{\partial (\tau_{ij})}{\partial x_j}, \tag{2}$$

$$\frac{\partial \overline{c}}{\partial t} + \frac{\partial (\overline{u}_j \overline{c})}{\partial x_j} = (\frac{\nu}{\sigma})\frac{\partial^2 \overline{c}}{\partial x_j \partial x_j} - \frac{\partial \gamma}{\partial x_j}, \tag{3}$$

where $u_i, \rho, p, \nu, c, \sigma$ denote the velocity, density, pressure, kinematic viscosity, passive scalar concentration, and laminar Schmidt numbers, and the strain rate tensor, $S_{ij} = \frac{1}{2}\left(\frac{\partial \overline{u}_i}{\partial x_j} + \frac{\partial \overline{u}_j}{\partial x_i}\right)$. Here $\sigma = 0.7$.

The terms $\tau_{ij} = \left(\overline{u_i u_j} - \overline{u}_i \overline{u}_j\right)$ in equation (2) and $\gamma = (\overline{u_j c} - \overline{u}_j \overline{c})$ appearing in equation (3) result from the unresolved sub-grid scale contributions and hence subsequent modeling is required to close the filtered momentum equations and filtered scalar equation. The Smagorinsky [28] eddy viscosity model is used to calculate the SGS stress tensor $\tau_{ij} = \left(\overline{u_i u_j} - \overline{u}_i \overline{u}_j\right)$ such that

$$\tau_{ij} - \frac{1}{3}\delta_{ij}\tau_{kk} = -2\nu_{sgs}\overline{S}_{ij} \tag{4}$$

and the SGS scalar flux $\gamma = (\overline{u_j c} - \overline{u}_j \overline{c})$ such that

$$\gamma = \frac{-\nu_{sgs}}{\sigma_t}\frac{\partial \bar{c}}{\partial x_j} \tag{5}$$

The eddy viscosity ν_{sgs} is given as a function of the filter size and strain rate

$$\nu_{sgs} = C_s \bar{\Delta}^2 \left|\bar{S}\right| \tag{6}$$

where C_s is a Smagorinsky [28] model parameter and $|\bar{S}| = (2\bar{S}_{ij}\bar{S}_{ij})^{\frac{1}{2}}$. Here we employed the localised dynamics procedure of Piomelli and Liu [29] to obtain the subgrid scale turbulent Schmidt number (σ_t) and the model parameter C_s appearing in equations (5) and (6).

3. SIMULATION DETAILS

3.1. Numerical discretisation methods

The mathematical formulations for mass, momentum and passive scalar are numerically solved by means of a pressure based finite volume method using the large eddy simulation code PUFFIN developed by Kirkpatrick et al. [30-31]. The code has been recently parallelised by Kirkpatrick [32] and the results presented in this paper have been obtained using the parallel version. Spatial discretisation is achieved using a non-uniform Cartesian grid with a staggered cell arrangement. Second order central differences (CDS) are used for the spatial discretisation of all terms in both the momentum equation and the pressure correction equation. The diffusion terms of the passive scalar transport equation are also discretised using the second order CDS. The convection term of the passive scalar transport equation is discretised using a third order QUICK with ULTRA flux limiter [33] to ensure that the solution remains monotonic.

The momentum and scalar transport equations are integrated in time using a hybrid second order Adams-Bashforth/Adams-Moulton scheme. The pressure correction method of Van Kan [34] and Bell et al. [35] which involves solving an equation for pressure correction rather than the pressure is used for the present work. The solution to this equation is then used to project the approximate velocity field that results from the integration of the momentum equations onto a subset of divergence free velocity fields. The time step is varied to ensure that the maximum Courant number $C_o = \Delta t u_i / \Delta x_i$ remains approximately constant where Δx_i is the cell width, Δt is the time step and u_i is the velocity component in the x_i direction. The solution is advanced with time steps corresponding to a Courant number in the range of $C_o = 0.3$ to 0.5. A Gauss-Seidel solver is used to solve the system of algebraic equations resulting from the numerical discretisation of momentum and passive scalar transport equations. The BiCGStab method with a Zebra Gauss-Siedel preconditioner using successive overrelaxation (SOR) and Chebyshev acceleration is used to solve the algebraic equations resulting from the discretisation of pressure correction equation.

3.2. Computational geometry, domain, and boundary conditions

The simulated round jet configuration has been studied experimentally by Garry and Holt as a part of a wider investigation of initial jet mixing relevant to the environmental impacts of aircraft engine efflux [36]. Their investigation considered a single, $D = 6.35mm$ diameter jet, with bulk exit velocity of 23 m/s and free-stream velocity of 5 m/s, to which a neutrally buoyant gas was added. In addition, they also considered a jet with a circular bluff body at the inlet plane with diameters $D_1 = 25mm$ and $D_2 = 50mm$ respectively. Our simulations for all three configurations employed a non-uniform Cartesian grid covering the full range of experimental

measuring stations extending 210 jet diameters (D) axially and 25D radially, with a 2.4 million point grid distributed as $240(axially)\times100\times100$. Fig. 1 (a-c) show the LES snapshots of filtered axial velocities for round jet, round jet with circular bluff body of diameter $D_1 = 25mm$ and round jet with circular bluff body of diameter $D_2 = 50mm$. Each figure contains marked axial locations which have been considered for intermittency calculation.

The inlet jet nozzle mean velocity distributions were specified using a standard $1/7^{th}$ power law velocity profile:

$$U_{jet} = U_{bulk} C(1 - r/r_{jet})^{\frac{1}{7}} \tag{7}$$

Here the constant C=1.32 is consistent with a fully developed turbulent pipe flow condition upstream of the nozzle exit. An appropriate, 10% turbulence intensity was imposed by superimposing fluctuations on the mean velocity profiles generated by a Gaussian random number generator. A free slip boundary condition was applied to the domain walls (except for a case in which a solid wall was substituted at the lower boundary surface). The upstream boundary was specified as a multiple inlet; while at the downstream outlet, a zero normal gradient boundary was employed.

The simulations have been carried out in both serial and parallel environments, with the computational grid distributed over to up to 10 processors using axial direction partitioning on the Cranfield HP Supercomputer, Astral.

4. RESULTS, ANALYSIS AND DISCUSSION

This section presents a detailed description of the computed pdf distributions and radial variation of intermittency fields for velocity and passive scalar for the round jet, round jet with circular bluff body of diameter D_1 and round jet with circular bluff body of diameter D_2. However, since validation of the LES predicted velocity and passive scalar fields is necessary before we can discuss any physical insights obtained regarding turbulent intermittency, first we discuss the comparison between LES results and experimental measurements for the round jet. Subsequent sections discuss the computed probability density functions and external intermittency profiles of both velocity and passive scalar fields at different axial and radial locations.

4.1. Time-averaged calculations

Fig. 2 (left-hand side) shows the resulting LES predictions for the mean velocity field at different axial locations compared to experimental measurements. It can be seen that the streamwise mean velocity profile development, both in magnitude and shape, is in good agreement with that measured throughout nearly the whole of the flow domain. There is just a small underprediction of the centreline value at 15 and 30D, which may indicate a need for preferentially higher axial grid resolution where such rapid variations are occurring in the stream direction.

The distribution of the rms (root mean square) axial velocity is also seen to be correctly reproduced by the simulations in Fig. 2 (right-hand side), but their peak magnitude is somewhat overpredicted. This is not inconsistent with the use of a simple turbulence eddy viscosity sub-grid scale modelling and may well reflect the need for intermittency-scaling of the sub-grid scale contribution and for which it is

necessary to study the intermittency for both the velocity and scalar near and far fields.

A comparison of the LES results and experimental data for the mean passive scalar field is shown in Fig. 3. In this case, the experimental data was limited to a smaller axial range of stations due to difficulties detecting the jet efflux tracer gas in the far field. However it appears that the width and therefore spreading rate of the scalar is particularly well captured by the LES.

4.2. Intermittency field studies

4.2.1 Intermittency calculation

The physical interpretation of intermittency can be divided into two parts namely external intermittency and internal intermittency. The interfacial distinction between turbulent-bearing fluid (e.g. the jet or the boundary layer) and non-turbulent fluid (free stream) is referred as the external intermittency. Internal intermittency refers to local fluctuations of turbulence intensity (the intermittency in an inertial range of a turbulent flow). Both external and internal intermittency can be seen as multiscale spatiotemporal random processes. Mathematically external intermittency can be expressed using an indicator function with the value of one in turbulent regions and zero in non-turbulent (laminar) regions. The indicator function represents the fraction of the time interval during which a point is inside the turbulent fluid.

Generally, a statistical tool is required for the external intermittency calculation and the probability density function (pdf) plays an important role in this regard. For example, a normalised histogram method tested by Andreotti and Douady [37] can be

used to determine the pdf. Thus the intermittency value can be calculated using a summation of probability values for a given threshold value

Since various techniques are available to calculate external intermittency, here we employed two approaches – the first method based on previous computational studies and the second method based on experimental studies. The first method was originally proposed by Schefer and Dibble [6]. In their method, the intermittency for a particular variable can be calculated from pdfs in which we assumed that the pdf is smooth at the scale of one histogram bin. In our investigation we considered 8000 measurements at each spatial location with 50 bins over $3-\sigma$ limits of data are considered. Therefore the normalised PDF's can be written as

$$\int_0^1 P(f)df = 1 \tag{8}$$

The intermittency value γ (gamma) can be calculated from the probability values with respect to considered threshold value such that

$$\gamma = P(f > f_{th}) \tag{9}$$

The second method, which chooses the fluctuation of the variable (for example velocity fluctuation in velocity intermittency calculation), is an approach more widely used by many experimental investigations. Here the intermittency factor is defined as the fraction of time that the fluctuation of the variable itself is greater than a threshold. For any variable ϕ, the flow is considered to be turbulent if the fluctuation $|\phi'| > \phi_{th}$. The ratio of the time the flow is turbulent to the total time then provides the intermittency factor.

4.2.2 Intermittency of a jet

This section discusses the probability density function (pdf) distributions and radial variation of intermittency first for the axial velocity and then for the passive scalar. The pdf distributions of the axial velocity at equidistant radial locations (r/D=0.0, 1.0, 2.0 and 3.0) at axial location x/D=20 are presented in Fig. 4. As seen in Fig. 4 (r/D=0.0), the evolution of the pdf on the jet centreline exhibits a Gaussian like distribution. However the pdf shape becomes less well structured with increased radial distance and shifts towards a delta function at the furthest radial locations, see Fig. 4 (r/D=3.0). The intermediate region Fig. 4 (r/D=1.0,r/D=2.0) can be identified as a highly intermittent region where we can assume less structured pdf distributions occur because of frequent changes from rotational to irrotational velocity fluctuations.

The radial profiles of the axial velocity intermittency calculated for two different threshold values based on method 1 are shown in Fig. 5. Since the axial velocity of the jet in the co-flow lies between 5 m/s and 23 m/s we chose to employ two threshold values of $u_{th} = 5.1, 6.1$ m/s in the first method for the analysis of threshold sensitivity. As seen in Fig.5 the intermittency values show little difference, however, the laminar region shifts more towards the centreline (as indicated by zero intermittency values) as a result of the higher threshold value.

Fig.6. shows the velocity intermittency profiles calculated using methods 1 and 2. Since we already compared the sensitivity of the threshold for method 1 (Fig.5), here we have used a threshold of $u_{th} = 6.1 m/s$. In method 2 we selected a threshold for the axial velocity fluctuation $u' = 0.5 m/s$ typically used for the experimental studies, namely approximately 10% of the peak value. The calculated profiles for the near

field (x/D=10, 20) and far field (x/D=30, 40) axial locations show the variation of intermittency for corresponding methods and threshold values. Although we could get similar values for intermittency with both methods by adjusting threshold values, our intention here is to demonstrate the prediction of external intermittency using two noted methods for selected thresholds values.

The pdf distributions of the passive scalar at an axial location x/D=20 are shown in Fig. 7. A similar method to that discussed in the velocity intermittency section was again applied to determine the probability density functions of the scalar. Fig.7 (r/D=0.0) shows the variation of the pdf on the centreline which indicates a Gaussian type distribution. Again, pdf shapes become more irregular at intermediate regions, Fig. 7 (r/D=1.0, r/D=2.0) and then shift to a delta function at the furthest radial location, Fig. 7 (r/D=3.0).

Fig.8 shows passive scalar intermittency profiles at axial locations x/D=10, 20, 30 and 40 obtained from two different threshold values $f_{th} = 0.05$ and 0.06 using method 1 [6]. The comparison indicates the laminar region (zero intermittency value) at a lesser radial distance for the higher threshold value. The comparisons of the passive scalar intermittency obtained from methods 1 and 2 are shown in Fig. 9. The first method again used the Schefer and Dibble [6] technique with threshold value of $f_{th} = 0.06$ while the second method considered the passive scalar fluctuation with a threshold value of $f' = 0.01$ which is close to 10% of the peak variance. It is interesting to note that both methods demonstrate similar variation of intermittency at near field axial locations (x/D=10, 20, 30) for the considered threshold values. However, in addition to these findings it is also important to make a comment about the variation of the

presented scalar intermittency results with respect to available experimentally based intermittency findings. Despite using different threshold values, our analysis indicated good consistency for the distribution of passive scalar intermittency with the results of Schefer and Dibble [6]. Furthermore, the decay is similar at near field axial locations and the differences only become large in the far field region. Therefore the present findings certainly add a new dimension to the available intermittency literature especially for the round jet.

4.2.3 Intermittency of a jet with bluff body

To relate pdfs and intermittency findings for the round jet to more complex recirculating flows similar to practical engineering applications requires further analysis. In this section we fulfil the second objective of the work and discuss the variation of pdfs and external intermittency in the presence of near field flow recirculation zone formed by a circular bluff body. The objective of introducing a circular bluff body is to study the variation of external intermittency due to the torroidal shaped recirculation zone formed by the sudden expansion at the bluff body wall. Here we consider two different bluff body diameters and results will be analysed for the variation of intermittency of both velocity and passive scalar in the presence of different sized torroidal recirculation zones compared to the jet.

A comparison of velocity pdfs for a jet with and without a bluff body at equidistant radial locations r/D=0.0, 1.0, 2.0 and 3.0 at x/D=20 is shown in Fig.10. The differences between the pdfs of velocity are wider near the centreline due to the formation of the recirculation zone for the bluff body jets, but show similar behaviour at the furthest radial locations. The Gaussian type distribution is seen near the

centreline also for the bluff body jets and eventually converts into a delta function at furthest radial locations. The differences between the pdfs of velocity near the centreline provide an indication of the intermittent behaviour associated with the bluff body stabilised recirculation zone. As seen in Fig.11 the pdfs of the passive scalar also show differences close to the jet centreline and follow a similar behaviour to the velocity field. The changes in the bluff body diameter (D_1 and D_2) affect the size of the recirculation zone and hence the variation in pdfs of both velocity and scalar fields and thus we can expect deviation of the intermittency value with respect to the jet for a given threshold value.

Fig.12 shows the radial profiles of velocity intermittency at x/D=10, 20 and 30. Here we used the threshold value of $u_{th} = 6.1 m/s$. As expected, the variation of the intermittency values indicates the effect of the bluff body on velocity intermittency with respect to a given threshold value. The introduction of a recirculation zone due to a circular bluff body reducdes the intermittency value on the centreline in the near field and thus indicates the variation of turbulence fluctuations. However, the radial profiles for all three cases follow the similar shape distribution in the near field (x/D=10) and start to deviate in the intermediate region (x/D=20) and also at the downstream limit of the bluff body stabilised recirculation zone (x/D=30). As seen in Fig.12 (x/D=30.0), the velocity intermittency shows rapid variation with respect to bluff body diameter which changes the axial extent of the recirculation zone. Therefore the velocity intermittency profile provides useful details for the variation of intermittency for a round jet with and without a circular bluff body.

The radial profiles of scalar intermittency at x/D=10, 20 and 30 are shown in Fig.13. Here we used a threshold value of value of $f_{th} = 0.06$. The scalar intermittency profiles shows similar variation at all three axial locations with slight differences apparent at x/D=10 and 20.

We believe that the comparison plots of pdf distributions and intermittency of the turbulent round jet for both velocity and passive scalar, with and without a torroidal shaped near field recirculation zone provide contributions to the established literature that are of both intrinsic and practical value. Methodology and data established in the present investigation could be used to determine the characteristic features of active scalars especially in combustion applications. The present findings are particularly relevant to bluff body stabilised flames in both premixed and non-premixed combustion applications, and thus could also potentially be used to analyse instantaneous behaviour of active scalars in the context of large eddy simulation. Since we used the dynamics sub-grid LES model the variation of intermittency with respect to inlet conditions provides further useful input concerning the instantaneous flow characteristic in the presence of a wall surface and so provides additional detail of near wall behaviour. Therefore the results discussed here could also be helpful for near wall sub-grid model development.

There are number of other important issues identified in this investigation which should be considered for a next phase of investigation. A natural continuation of the present work is the study of intermittency by solving an intermittency transport equation. In particular, it would be instructive to solve a modified intermittency transport equation in the LES sub-grid scale modelling that has been originally

developed in a RANS context [26]. An intermittency factor could simply be included into Smagorinsky eddy viscosity model once determined from the intermittency transport equation. Alternatively however, a dynamic Smagorinsky model could be considered in which the degree to which the large scale space filtering could be determined using local box estimation directly. This then can be used to calculate effect of intermittency on sub-grid scale eddy viscosity. It is well known that the LES sub-grid models assume the existence of a cascade process and therefore sub-grid scale physical process conditioned from the resolved scale physical process depend on the filtered scale. However, the cascade process might not completely valid for high Reynolds number free shear flows where we experience high intermittency behaviour especially in the region of a viscous super layer. In such situations, an alternative modelling strategy such as a level set approach perhaps could be useful and thus also needs to be considered in future modelling.

5. CONCLUSIONS

This paper has presented modelling of turbulent intermittency of high Reynolds number round jets using a large eddy simulation technique. First the accuracy of the numerical results was tested with available experimental data and then analysed for the intermittent variation from turbulent to laminar flow for both velocity and passive scalar fields.

Generally, our LES results are in good agreement with experimental data for both velocity and passive scalar fields. The axial decay and radial spread of the axial velocity and passive scalar are found to closely match the experimental results.

Having established the accuracy of the LES results, investigation was then further extended to analyse the intermittent behaviour of the jet flow with and without a bluff body using the LES database. Derived probability density function distributions for both velocity and passive scalar indicate these change from Gaussian distributions to a delta function with increased radial distance. The intermittency factor calculated using two different methods shows similar variation at different axial locations and different threshold values demonstrate the regional changes between turbulent and laminar values. Adding a circular bluff body to a jet changes the structure of the pdfs for both velocity and passive scalar fields. In particular, the intermittency values of velocity indicate differences in the near field close to the jet centreline and also close to the downstream limit of the recirculation zone.

In this study we have employed a standard dynamic sub-grid model without inclusion of any specific allowance for such intermittency effects. Further work is necessary to include the effects of intermittency on the sub-grid modelling of large eddy simulation, which should improve sub-grid models for the application of LES to such inhomogeneous free shear flows.

Acknowledgment: We are grateful to the EPSRC for their financial support under grant EP/E036945/1 on the Modelling and Simulation of Intermittent Flows. We also acknowledge the computing time provided by Cranfield Astral HPC.

REFERENCES

[1] Warhaft Z. Passive scalars in turbulent flows. Annu Rev Fluid Mech 2000; 32, 203-240.

[2] Townsend AA. Local isotropy in the turbulent wake of cylinder. Austr J Sci Res 1948; 1, 161-168.

[3] Becker HA, Hottel HC, Williams GC. Concentration intermittency in jets. Tenth Symp Combut , The Combust Inst, 1965.

[4] Wygnanski I, Fiedler HE. Some measurements in the self preserving jet. J Fluid Mech 1969; 38, 577-612.

[5] Bilger RW, Antonia RA, Sreenivasan KR. Determination of intermitency from the probability density function of a passive scalar. Phys Fluids 1976; 19 (10), 1471-1474.

[6] Schefer RW, Dibble RW. Mixture fraction field in a turbulent nonreacting propane jet. AIAA J 2001; 39, 64-72.

[7] Libby PA. On the prediction of intermittent turbulent flows. J Fluid Mech 1975; 68, 273-279.

[8] Dopazo C. On conditioned averages for intermittent turbulent flows. J Fluid Mech 1977; 81, 433-445.

[9] Chevray R, Tutu NK. Intermittency and preferential transport of heat in a round jet. J Fluid Mech 1978; 88, 133-145.

[10] Boersma, BJ, Brethouwer G, Nieustadt FTM. A numerical investigation of the effect of the inflow conditions on a self-similar region of a round jet. Phy. Fluids 1998; 10 (4), 899-909.

[11] Freund JB, Lele SK, Moin P. Direct numerical simulation of a supersonic round turbulent shear layer. AIAA paper 1997; 97-0760.

[12] Lubbers CL, Brethouwer G, Boersma BJ. Simulation of the mixing of a passive scalar in a round turbulent jet. Fluid Dyn Res 2001; 28, 189-195.

[13] Babu PC, Mahesh K. Upstream entrainment in numerical simulations of spatially evolving round jets. Phy Fluids 2004;16(10), 3699-3705.

[14] Babu PC, Mahesh K. Direct numerical simulation of passive scalar mixing in spatially evolving turbulent round jets. AIAA Paper 2005; 1121.

[15] Lesieur M, Metais O. New trends in large eddy simulations of turbulence. Annu Rev Fluid Mech 1996; 28, 45-82.

[16] Piomelli U. Large eddy simulation: achievements and challenges. Prog Aero Sci 1999; 34(4), 335-362.

[17] Mankbadi RR, Hayder ME, Povinelli LA. Structure of supersonic jet flow and its radiated sound. AIAA J 1994; 32(5), 897-906.

[18] Boersma BJ, Lele SK. Large eddy simulation of a Mach 0.9 turbulent jet. AIAA 1999; 99-1874.

[19] Yuan LL, Street RL, Ferziger JH. Large eddy simulation of a round jet in cross flow. J Fluid Mech 1999; 379, 71-104.

[20] Byggstoyl, S, Kollmann W. Closure model for intermittent turbulent flows. Int J Heat Mass Transfer 1981; 24, 1811-1818.

[21] Kollomann W, Janicka J. The probability function of a passive scalar in turbulent shear flows. Phy Fluids 1982; 25(10), 1755-1769.

[22] Cho JR, Chung MK. A $k-\varepsilon-\gamma$ equation turbulence model. J Fluid Mech 1992; 237, 301-322.

[23] Dewan A, Arakeri JH, Srinivasan J. A new turbulence model for the axisymmetric plane. J Appl Math Model 1997; 21, 709-791.

[24] Kalita K, Dewan, A, Dass AK. Computation of the turbulent plane plume using the model. J Appl Math Model 2000; 24(11), 815-826.

[25] Pope SB. Calculation of plane turbulent jet. AIAA J 1984; 22(7), 896-904.

[26] Savill AM. New Strategies in modelling bypass transition. Closure Staregies in Turbulent & Transitional Flows, Cambridge University Press Chapter 18, 2005.

[27] Alvani RF. Mathematical modelling of the ignition characteristics of flammable jets. PhD Thesis, University of Leeds, 2004.

[28] Smagorinsky J. General circulation experiments with the primitive equations. M Wea Review 1964; 91, 99-164.

[29] Piomelli, U. and Liu, J. Large eddy simulation of channel flows using a localized dynamic model. Phy Fluids 1995; 7: 839-848.

[30] Kirkpatrick MP, Armfield, SW, Kent JH. A representation of curved boundaries for the solution of the Navier-Stokes equations on a staggered three-dimensional Cartesian grid. J of Comput Phy 2003; 184: 1-36.

[31] Kirkpatrick MP, Armfield SW, Masri AR, Ibrahim SS. Large eddy simulation of a propagating turbulent premixed flame. Flow Turb Combust 2003; 70 (1): 1-19.

[32] Kirkpatrick, MP, Armfield, SW. On the stability and performance of the projection-3 method for the time integration of the Navier-Stokes equations. ANZIAM J 2008: 49: C559 –C575.

[33] Leonard BP, Mokhtari S. Beyond first order upwind: The ULTRA SHARP alternative for non-oscillatory steady-simulation of convection. Int J Num Meth Eng 1990; 30, 729-766.

[34] Van Kan J. A second order accurate pressure correction scheme fir viscous incompressible flow. SIAM J Sci Stat Comput 1986; 7, 870-891.

[35] Bell JB, Colella P, Glaz HM. A second order projection method for the incompressible Navier-Stokes equations. J Comput Phys 1989; 85, 257-283.

[36] Garry KP, Holt J. Modelling the dispersion of aircraft engine efflux in proximity to airports in an atmospheric boundary layer tunnel. Cranfield OMEGA Project Report, 2008.

[37] Andreotti B, Douady S. On probability distribution functions in turbulence. Part 1. A regularisation method to improve the estimate of a PDF from an experimental histogram. Physica D 1999; 132, 111-132.

FIGURE CAPTIONS

Fig.1. LES snapshot of the (a) round jet (b) round jet with a circular bluff body of diameter D_1 and (c) round jet with a circular bluff body of diameter D_2

Fig.2. Comparison of the mean (left-hand side) and rms (right-hand side) axial velocity. Lines represent LES results, and symbols represent experimental measurements

Fig.3. Comparison of the mean passive scalar. Lines represent LES results, and symbols represent experimental measurements

Fig.4. Velocity probability density function distributions at x/D=20 at equidistant radial locations r/D=0.0, 1.0, 2.0 and 3.0

Fig.5. Radial profiles for velocity intermittency at x/D=10, 20, 30 and 40. Circles represent method 1 with threshold value of 6.1 m/s and triangles represent method 1 with threshold value of 5.1 m/s

Fig.6. Radial profiles for velocity intermittency at x/D=10, 20, 30 and 40. Circles represent method 1 with threshold value of 6.1 m/s and inverted triangles represent method 2 with threshold value of 0.5 m/s

Fig.7. Passive scalar probability density function distributions at x/D=20 at equidistant radial locations r/D=0.0, 1.0, 2.0 and 3.0

Fig.8. Radial profiles for passive scalar intermittency at x/D=10, 20, 30 and 40. Circles represent method 1 with threshold value of 0.06 and triangles represent method 1 with threshold value of 0.05

Fig.9. Radial profiles for passive scalar intermittency at x/D=10, 20, 30 and 40. Circles represent method 1 with threshold value of 0.06 and inverted triangles represent method 2 with threshold value of 0.01

Fig.10. Comparisons of velocity probability density function distributions at x/D=20 at equidistant radial locations r/D=0.0,1.0,2.0 and 3.0. Here, solid lines denote jet results, dashed lines denote diameter D_1 bluff body stabilised jet and dotted lines denote larger diameter D_2 bluff body stabilised jet

Fig.11. Comparisons of passive scalar probability density function distributions at x/D=20 at equidistant radial locations r/D=0.0,1.0,2.0 and 3.0. Here, solid lines denote jet results, dashed lines denote diameter D_1 bluff body stabilised jet and dotted lines denote larger diameter D_2 bluff body stabilised jet

Fig.12. Radial profiles of velocity intermittency at x/D=10, 20 and 30. Here, circles denote jet results, squares denote diameter D_1 bluff body stabilised jet and inverted triangles denote larger diameter D_2 bluff body stabilised jet

Fig.13. Radial profiles of passive scalar intermittency at x/D=10, 20 and 30. Here, circles denote jet results, squares denote diameter D_1 bluff body stabilised jet and inverted triangles denote larger diameter D_2 bluff body stabilised jet

FIGURES

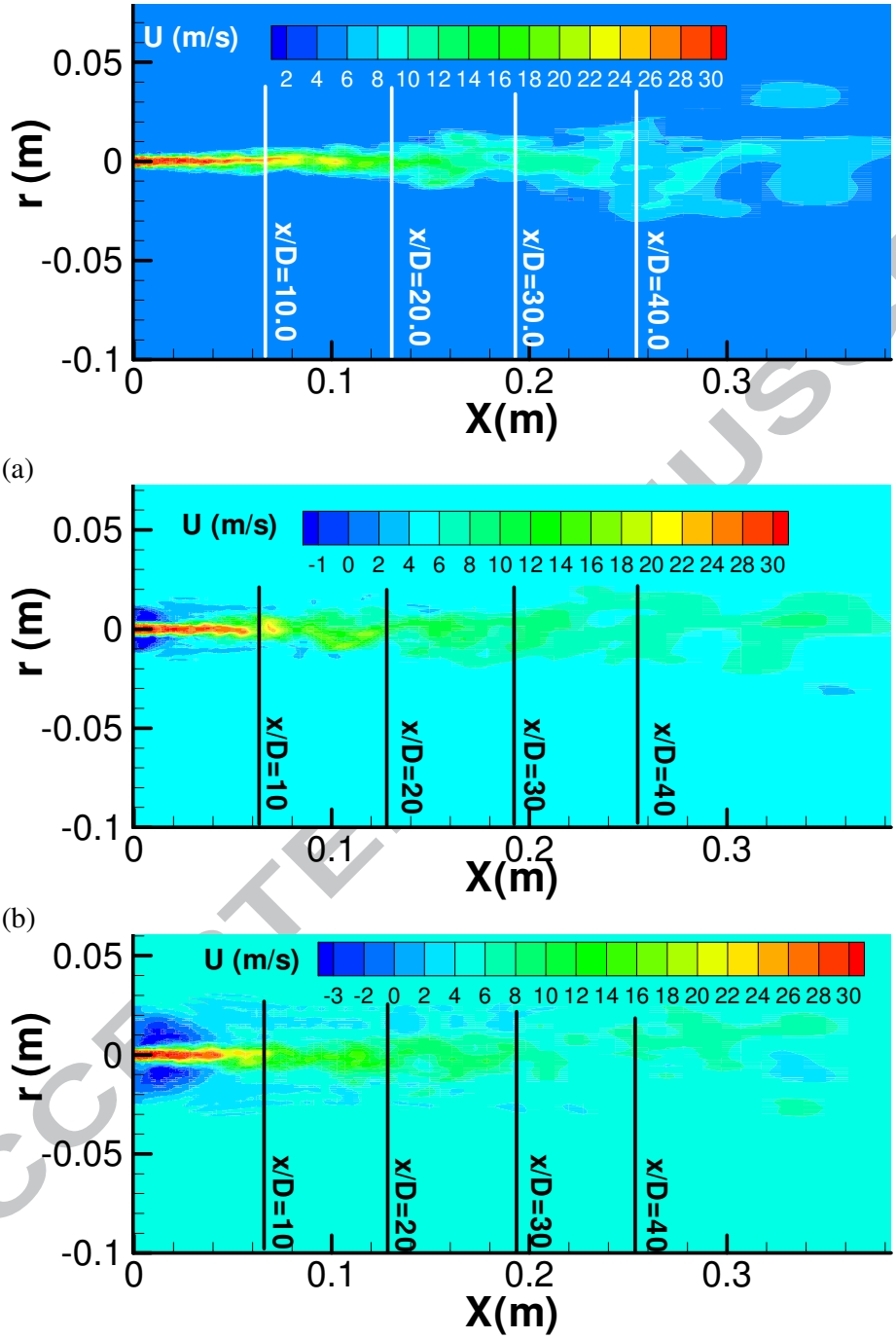

Fig.1. LES snapshot of the (a) round jet (b) round jet with a circular bluff body of diameter D_1 and (c) round jet with a circular bluff body of diameter D_2

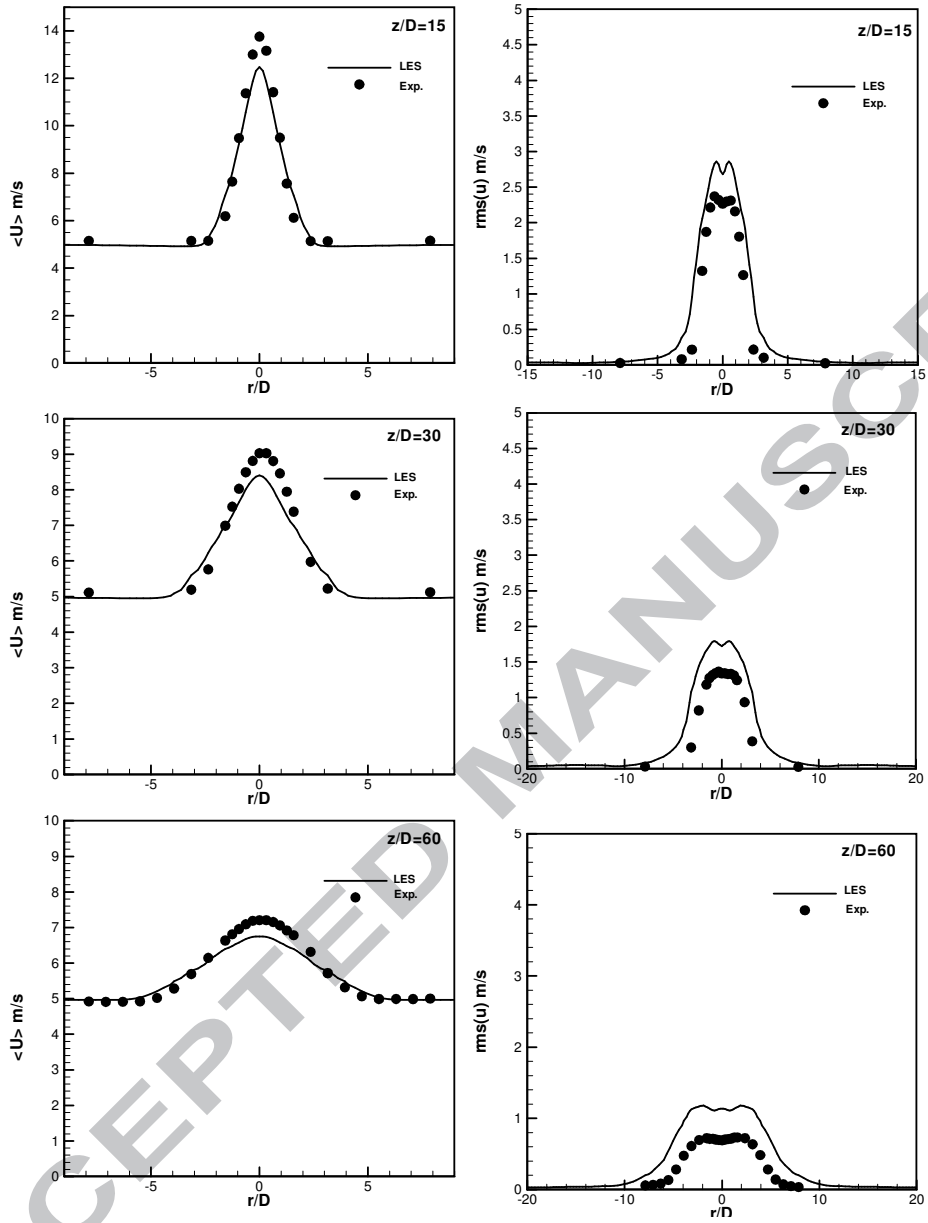

Fig.2. Comparison of the mean (left-hand side) and rms (right-hand side) axial velocity . Lines represent LES results, and symbols represent experimental measurements

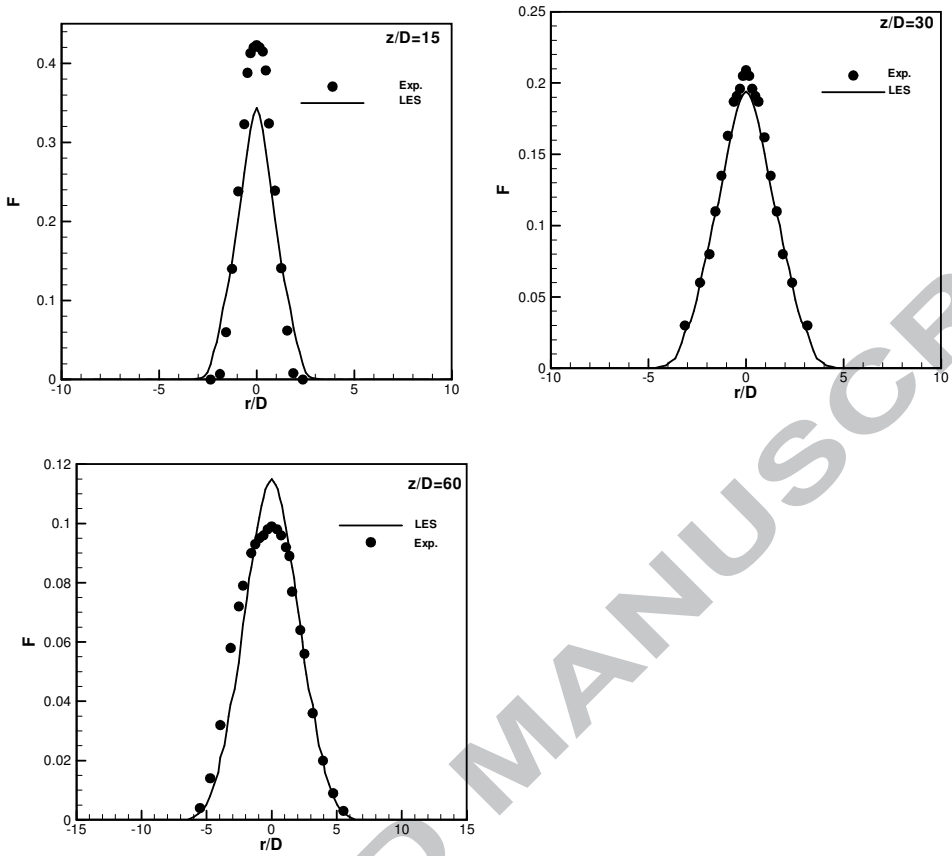

Fig.3. Comparison of the mean passive scalar. Lines represent LES results, and symbols represent experimental measurements

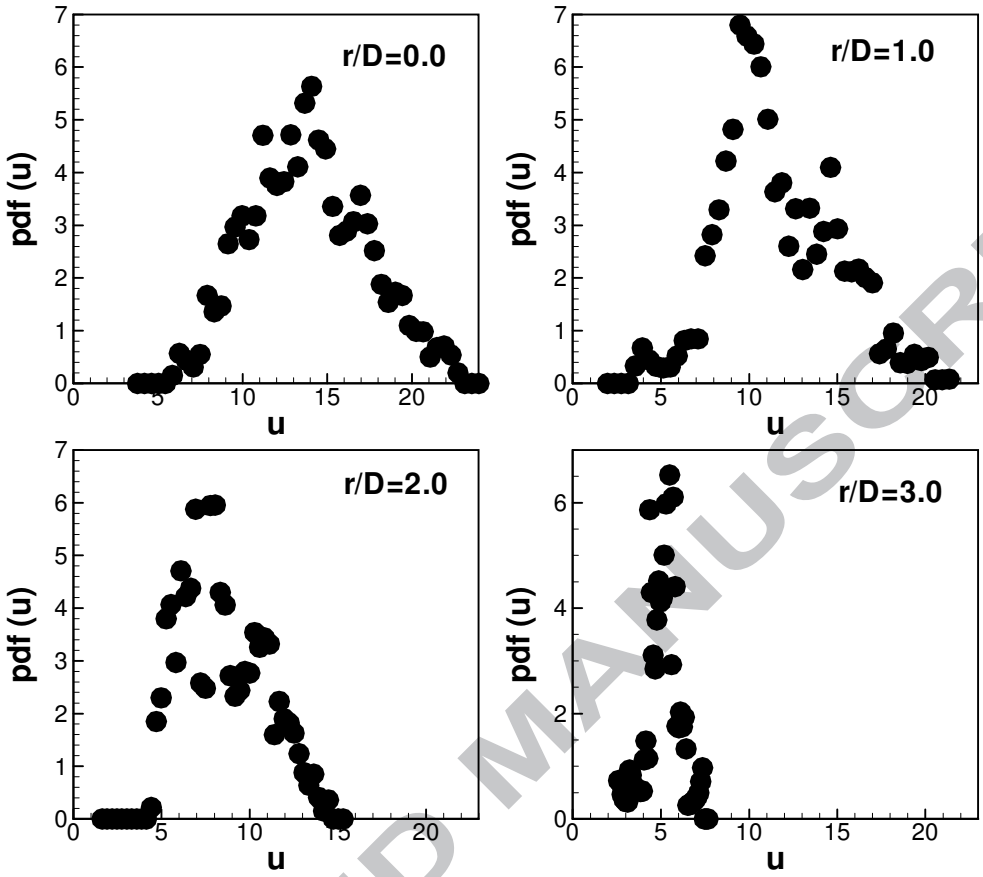

Fig.4. Velocity probability density function distributions at x/D=20 at equidistant radial locations r/D=0.0, 1.0, 2.0 and 3.0

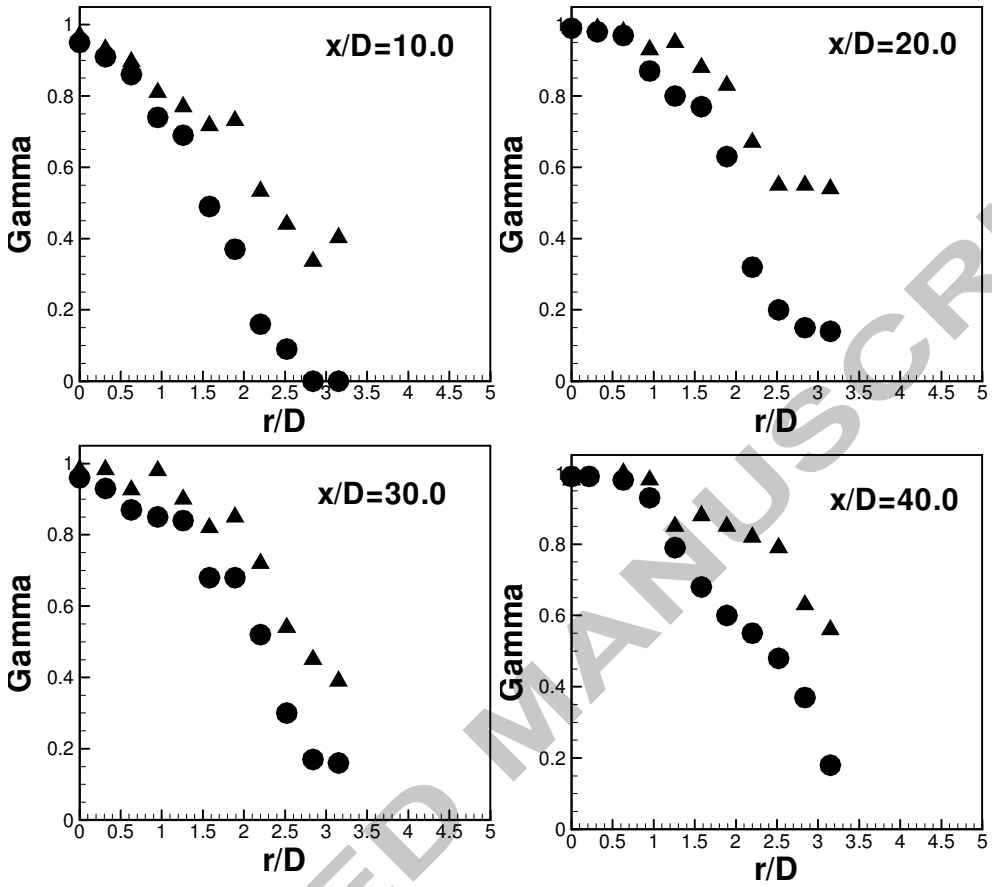

Fig.5. Radial profiles for velocity intermittency at x/D=10, 20, 30 and 40. Circles represent method 1 with threshold value of 6.1 m/s and triangles represent method 1 with threshold value of 5.1 m/s.

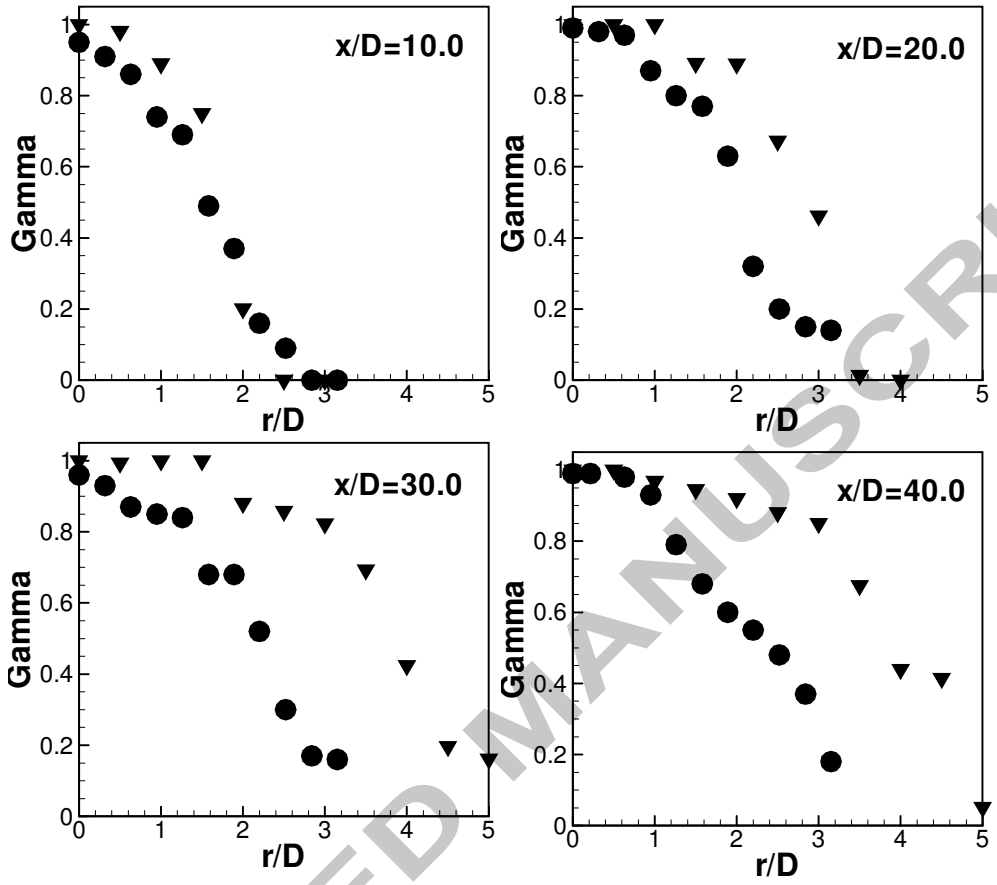

Fig.6. Radial profiles for velocity intermittency at x/D=10, 20, 30 and 40. Circles represent method 1 with threshold value of 6.1 m/s and inverted triangles represent method 2 with threshold value of 0.5 m/s.

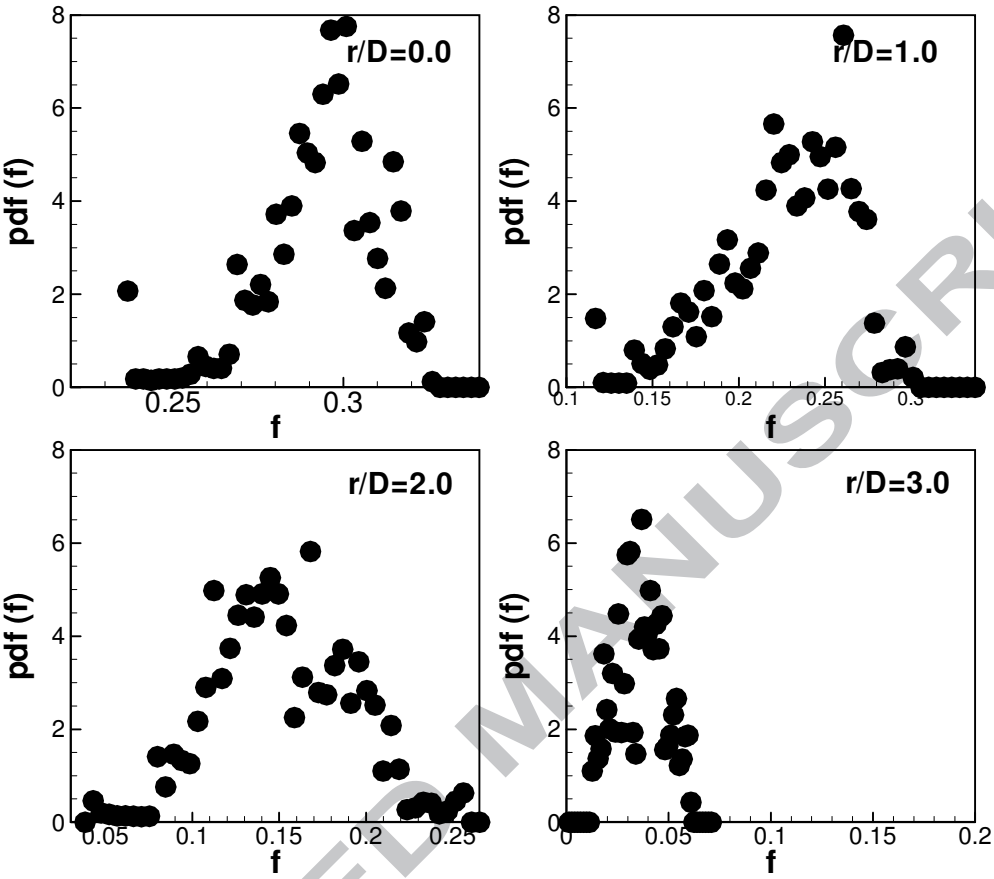

Fig.7. Passive scalar probability density function distributions at x/D=20 at equidistant radial locations r/D=0.0, 1.0, 2.0 and 3.0

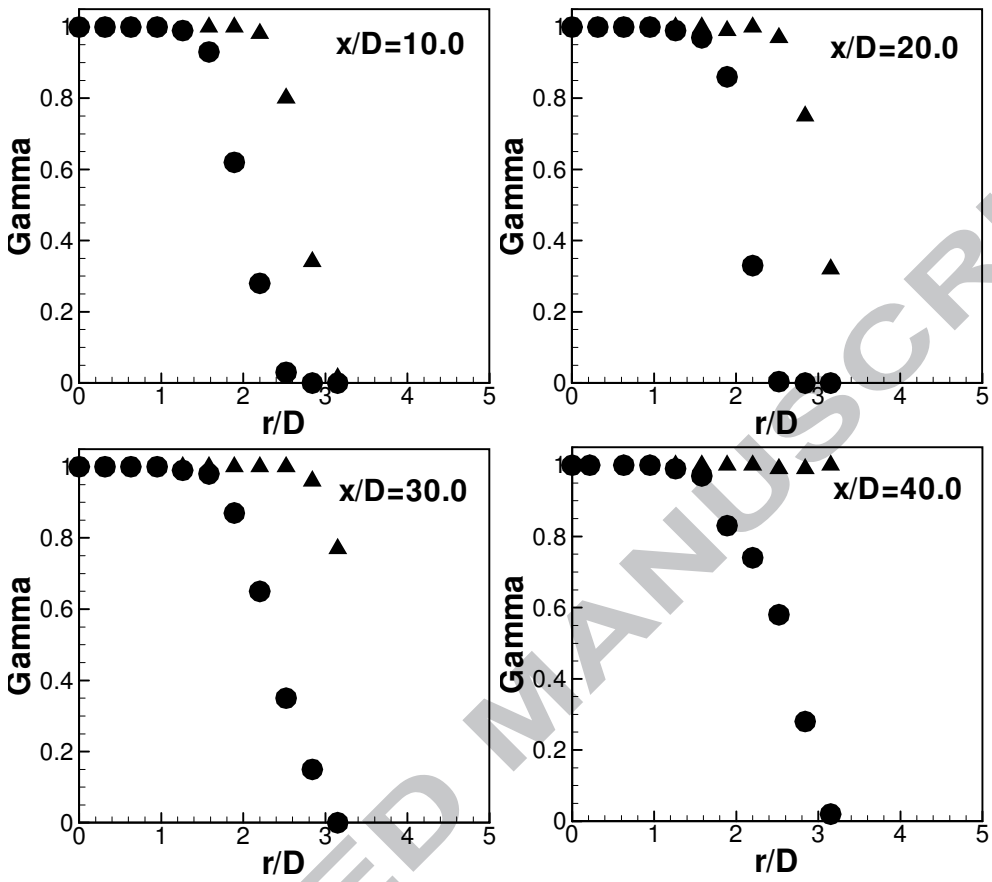

Fig.8. Radial profiles for passive scalar intermittency at x/D=10, 20, 30 and 40. Circles represent method 1 with threshold value of 0.06 and triangles represent method 1 with threshold value of 0.05

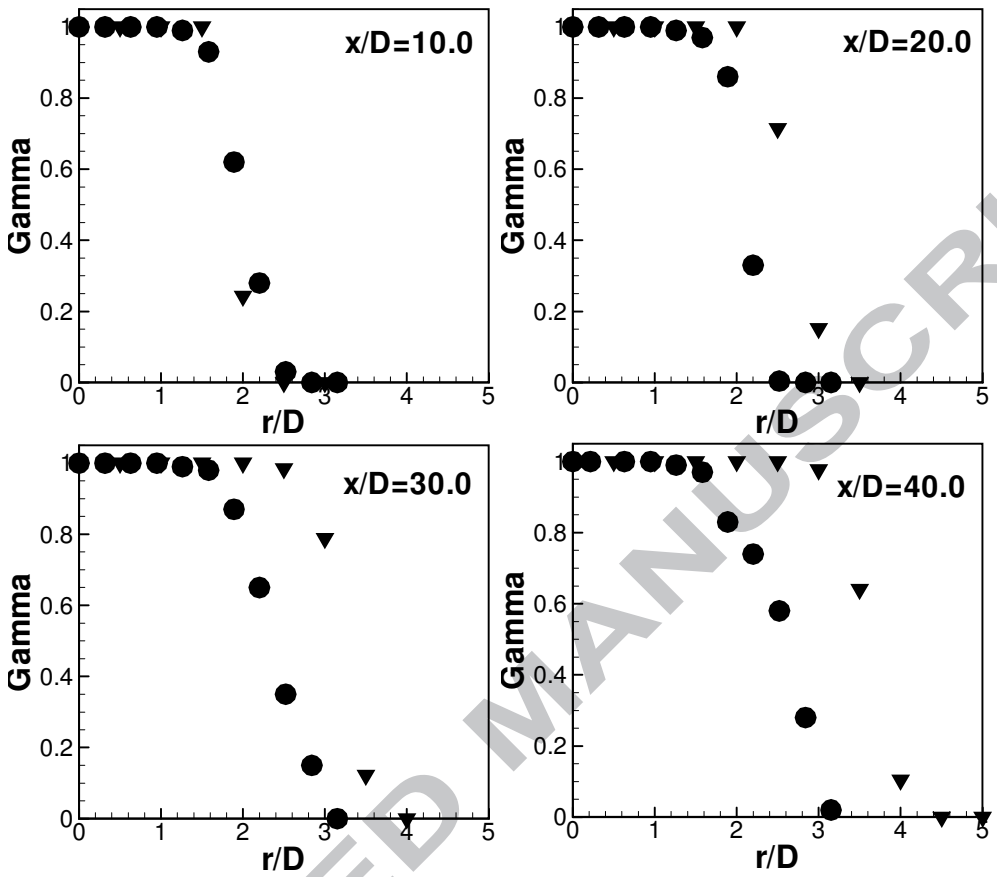

Fig.9. Radial profiles for passive scalar intermittency at x/D=10, 20, 30 and 40. Circles represent method 1 with threshold value of 0.06 and inverted triangles represent method 2 with threshold value of 0.01

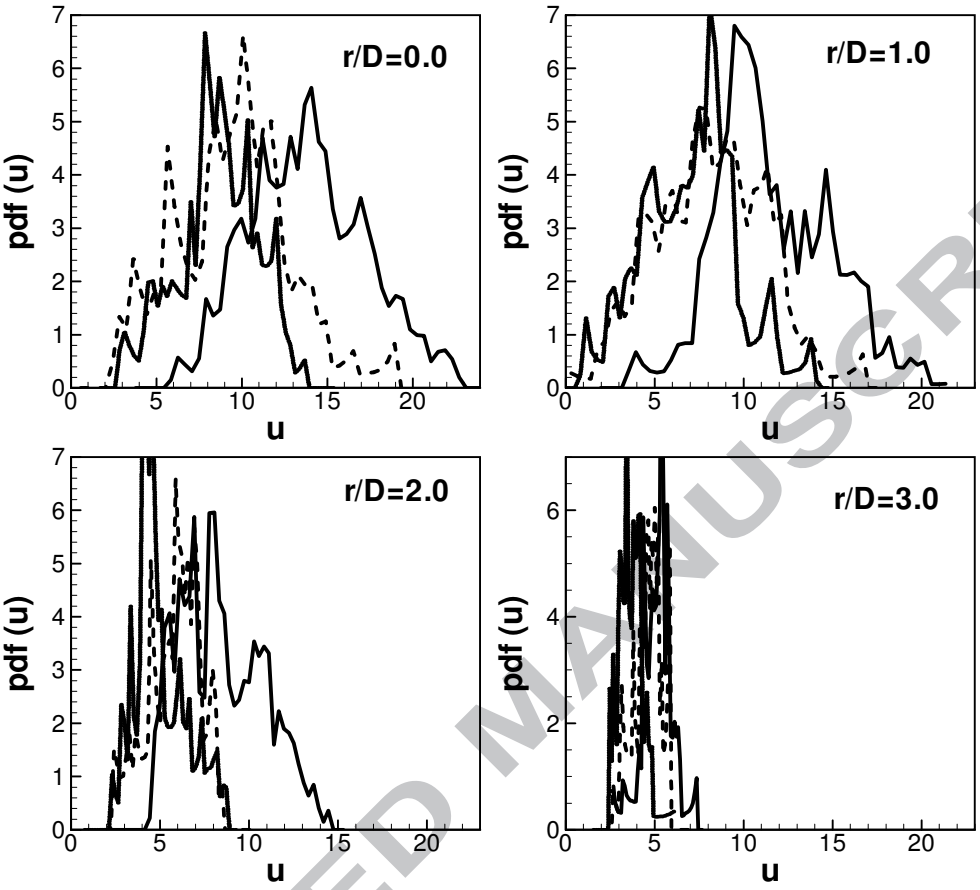

Fig.10. Comparisons of velocity probability density function distributions at x/D=20 at equidistant radial locations r/D=0.0,1.0,2.0 and 3.0. Here, solid lines denote jet results, dashed lines denote diameter D_1 bluff body stabilised jet and inverted dotted lines denote larger diameter D_2 bluff body stabilised jet.

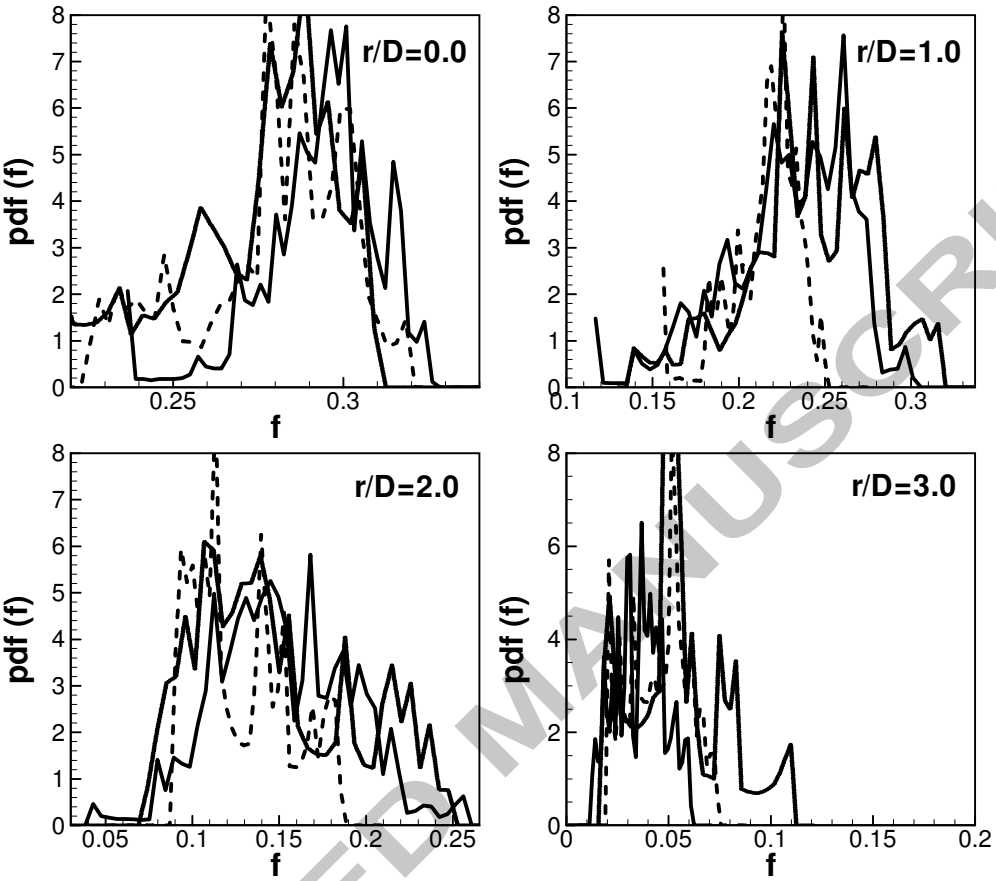

Fig.11. Comparisons of passive scalar probability density function distributions at x/D=20 at equidistant radial locations r/D=0.0,1.0,2.0 and 3.0. Here, solid lines denote jet results, dashed lines denote diameter D_1 bluff body stabilised jet and dotted lines denote larger diameter D_2 bluff body stabilised jet.

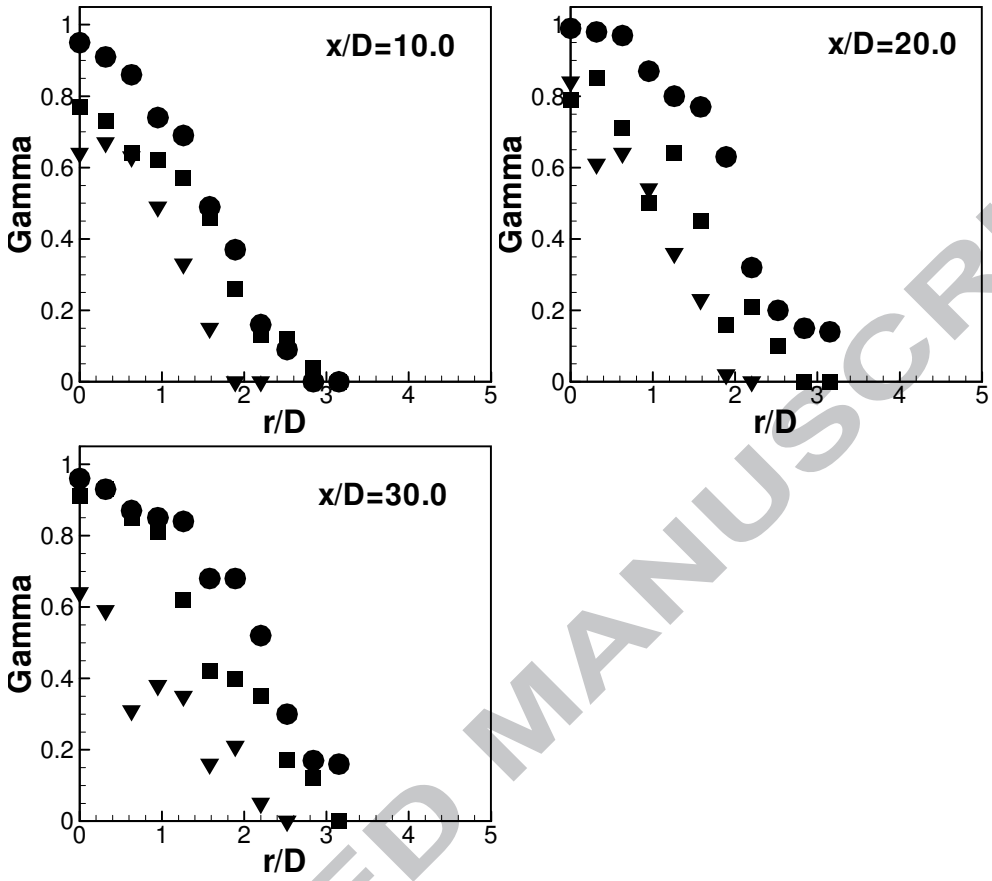

Fig.12. Radial profiles of velocity intermittency at x/D=10, 20, and 30. Here, circles denote jet results, squares denote diameter D_1 bluff body stabilised jet and inverted triangles denote larger diameter D_2 bluff body stabilised jet.

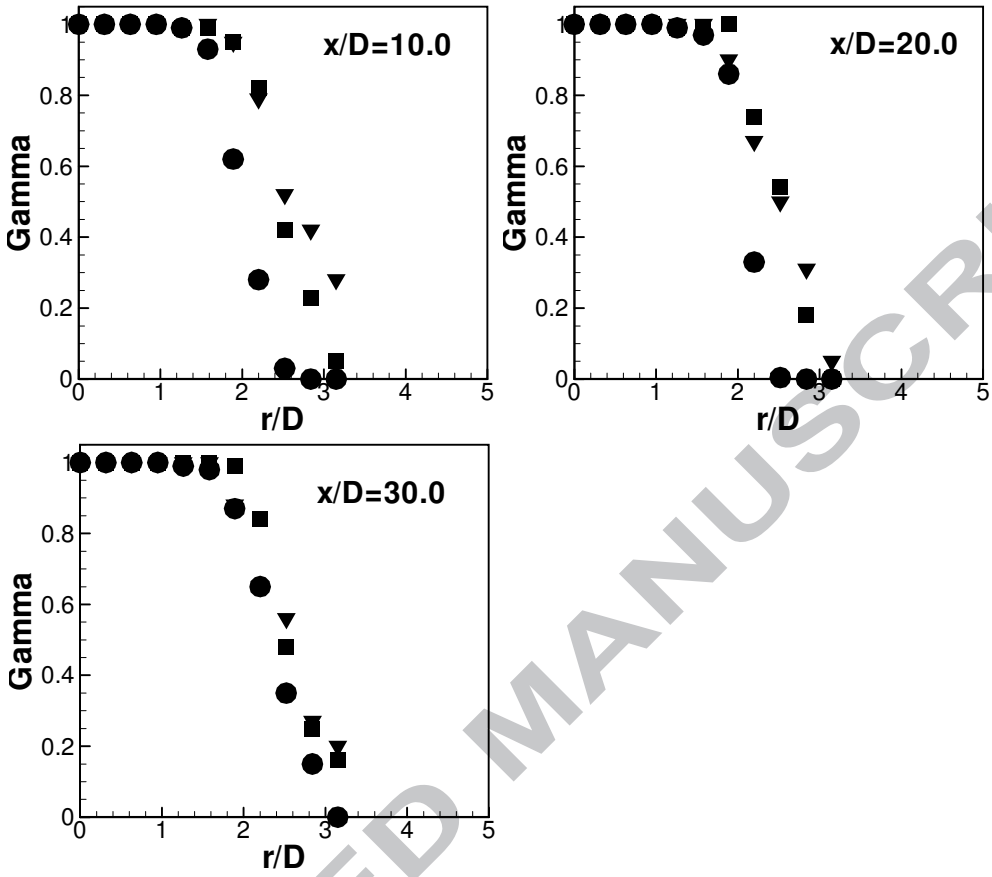

Fig.13. Radial profiles of passive scalar intermittency at x/D=10, 20, and 30. Here, circles denote jet results, squares denote diameter D_1 bluff body stabilised jet and inverted triangles denote larger diameter D_2 bluff body stabilised jet.